Nonlinear methods based on ultrasonic waves to analyse disbonds in single lap joints

G. Scarselli*[a], F. Ciampa[b], F. Nicassio[a], M. Meo[b]

[a]Department of Engineering for Innovation, University of Salento,

Via per Monteroni (Lecce), 73100, Italy

[b]Material Research Centre, Department of Mechanical Engineering,

University of Bath, Bath, BA2 7AY, UK

ABSTRACT

Adhesive bonded lap joints are widely used in the aerospace field and Non Destructive Testing (NDT) techniques are critical in evaluating the quality of adhesion before and during use. Two types of bonded samples have been experimentally investigated in order to verify the reliability of Nonlinear Elastic Wave Spectroscopy (NEWS) based on the use of ultrasound. Piezoelectric sensors have been attached to the samples and used as generators and receivers. Both the samples have shown nonlinearities in their dynamic behaviour. Nonlinear metrics have been applied to their structural responses over an assigned range of excitation frequencies based on higher order harmonic analysis in order to evaluate the degree of nonlinearity of the samples. Possible interpretations of the experimental behaviour are provided in the paper based also on tomographic testing of the adhesive layer that showed the presence of microbubbles in the bond due to manufacturing process.

Keywords: debonding, disbonds, damage detection, nonlinear elastic wave spectroscopy, Structural Health Monitoring

*gennaro.scarselli@unisalento.it: phone 0039 0832299720; fax 0039 0832299919; www.dii.unisalento.it

1. INTRODUCTION

Adhesives have been used to bond aircraft primary structures for over 60 years [1][2] and adhesion is currently widely used in aircraft manufacture as a direct alternative to riveting. The main uses of adhesives are bonding of stringers to skins for both fuselage and wing structures and of metallic honeycomb to skins for elevators, ailerons, tabs and spoilers. One of the major limiting factors in the use of adhesive bonding is the lack of a quantitative non-destructive technique able to detect and evaluate defects in the joint, particularly in the interfacial region between substrate and adhesive layer. Conventional NDT inspection techniques such as ultrasonics or X-ray [3]-[5] allow the detection of internal defects such as cracking, voids and porosity. However, conventional ultrasonic techniques are not so effective at detecting poor adhesion between the adhesive and the substrate as the thickness of this thin interfacial layer could be orders of magnitude less than the wave length used [6]. Numerous scientific literature sources evaluated in [7] clearly confirm that adhesive bond quality is a critical parameter that cannot yet be assessed by any NDT technique. Several conventional methods are suitable and have been improved for better detection capability but, to this day, no method can reliably and with a good reproducibility detect any weak adhesive bond, either on metal or composite substrates. Ultrasonic alternative methods (US spectroscopy, Nonlinear US, Guided Waves, Oblique incidence, Shear Wave Resonance and so on) as well as Laser Proof tests (LASAT, LBI, Laser Ultrasonic) and other methods like Shearography and Active Thermography are considered very effective and promising for the evaluation of adhesive bond quality. Those methods have already been applied to the characterization of delaminations, defects, or coating strength measurement in complex structures but each of them presents advantages and drawbacks when disbonds in adhesive joints have to be detected. Nonlinearities in a bonded joint can arise for different reasons: debonding can lead to clapping conditions resulting in contact acoustic nonlinearities and in a nonlinear load-displacement relation (Figure 1); when the ultrasonic waves travel through and/or are reflected from a weak adhesive layer (that can be associated to a nonlinear interface), they will be distorted by the interaction and this distortion will result, commonly, in harmonics of the input displacement signal with magnitudes clearly visible in the frequency domain. In Yan et al., the characteristics

of kissing bonds are investigated and ultrasound is employed to measure nonlinearity [8][9]. To accomplish this work, they prepared simple kissing bond samples (disbonds), using room temperature cure two-part epoxy. Perfectly bonded, fracture surface kissing bond, and contamination layer kissing bonds were produced. They used a high-frequency through-transmission technique and the nonlinearity associated with the kissing bond was measured from the distortion of the received signal under the action of low-level compressive loading. Nonlinearity decreased rapidly with compressive load. A nonlinear parameter β was defined as the ratio of the 2nd harmonic divided by the square of the fundamental frequency (the input signal frequency).

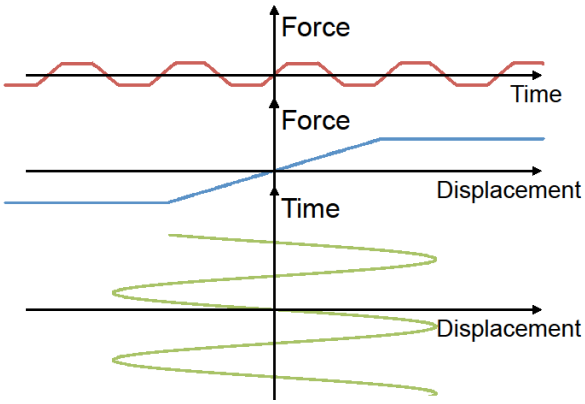

Figure 1. Nonlinearity induced by nonlinear load-displacement relation

The analyses of the experimental results showed that the nonlinear parameter β evaluated for the fracture surface specimen was higher than the reference and was significantly affected by contact pressure. This work confirmed that the measurement of nonlinearity allowed to detect effectively fracture surface kissing disbonds at low loading levels. Indeed through-transmission ultrasonic inspection cannot be considered readily field deployable on aircraft since it is typically based on the use of an elaborate “squirter” system to inspect structural components only after their removal from the aircraft. Yan et al. [10] concluded that, with the use of a one-dimensional time domain model, in which a nonlinear interface was defined to characterize the interaction of kissing bond and ultrasonic pulsing signals, the nonlinear parameter β was strongly affected by the thickness of the adhesive layer-to wavelength ratio and its variations could be due significantly to changes in adhesive geometry. Thus, they concluded that the employment of the metric β to characterize the

adhesive joint condition was valid when a reference was available: this could be a defect-free specimen with identical geometric and material properties or a numerical/analytical model. In [11] a combination of nonlinearity with Local Defect Resonance (LDR) enhanced substantially the efficiency of "conventional" nonlinear effects, like Higher Harmonics (HH) generation and frequency mixing, and resulted in qualitatively new "nonclassical" features characteristic of nonlinear and parametric resonances. According to the experiments, under LDR conditions the HH, frequency mixing and subharmonic components may dominate in vibration spectrum of defects. Both super- and subharmonic LDR were strongly localised in the defect area that provided a background for high-contrast defect-selective imaging.

Another possible source of nonlinearity in an adhesive layer is the presence of voids and cavities in the resin. Microbubbles containing gas and immersed in a liquid when radiated by an harmonic acoustic pressure field generate subharmonics and higher harmonics: the equation governing the microbubble dynamic behaviour is strongly nonlinear and has been widely investigated and solved with different boundary conditions [12][13]. In [14] the nonlinear response of bubbles to an acoustic field, resulting in sub- and super-harmonics, was used to accurately size and resolve the bubbles immersed in a liquid.

In this paper single lap joints (SLJs) made of aluminium plates bonded by epoxy resin adhesives are experimentally investigated, using Nonlinear Elastic Wave Spectroscopy. Two main configurations of SLJs were tested: fully bonded and partially bonded. Experiments have been performed feeding the exciting sensors attached to the samples with harmonic loading in the range between 10 kHz and 50 kHz. The structural response provided by the receiver sensors bonded onto the samples was found rich of subharmonics and higher order harmonics: because of the material adopted, the simple geometry, the boundary conditions and the electronic devices, the nonlinearities can be caused only by adhesion defects (clapping, kissing bond, voids in the adhesives).

2. MATERIALS AND METHODS

The geometry of tested samples and the experimental set-up are shown in the following Figure 2.

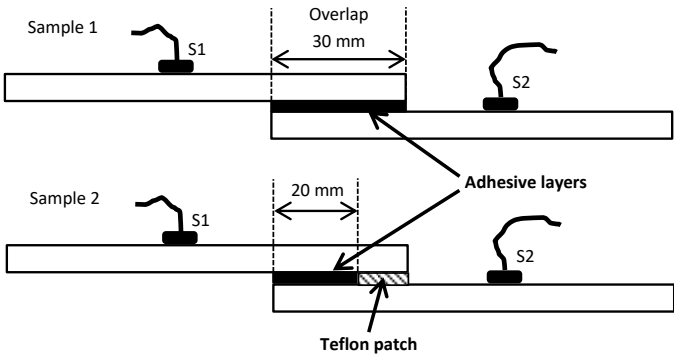

Figure 2a: specimens geometry

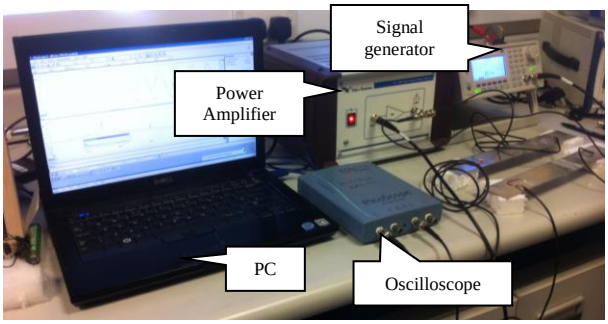

Figure 2b: the instrumentation

Figure 2. Test set-up

The simple specimens adopted for the experimental campaign were single lap joints made of two aluminum plates 2 mm thick, 42 mm wide, 145 mm long bonded with epoxy resin Araldite 320A: they are represented in Figure 2. In the Table 1 the materials properties are reported. One exciting sensor, S1, one receiving sensor, S2, were bonded onto the two samples: the sensors were piezoceramic discs with a diameter of 6 mm, 0.25 mm thick, with a resonant frequency of 8 MHz.

	Elastic modulus (GPa)	Density (kg/m^3)	Poisson modulus
Aluminum	71	2770	0.33
Araldite 320A	1.495	1220	0.33

Table 1: mechanical properties of the materials adopted for the specimens

It should be remarked that the nominal thickness of the adhesive layer was 0.15 mm: since the manual manufacturing process of the specimens did not allow a proper control of the adhesive layer thickness, it would be expected a discrepancy between the real and the nominal value. Two identical samples were manufactured, one labelled as Sample 1 (nominally fully bonded, to be used as a reference), the other one as Sample 2 (partially bonded). Artificial “disbond” was introduced in the Sample 2 bonding only 20 mm out the 30 mm of overlap: a Teflon patch 0.15 mm thick was placed between the two plates and, after the adhesive was completely set, the patch was removed. For the Sample 1, the two plates were bonded at all the overlap surface (see Figure 2a). During the experimental tests, a pure harmonic voltage was sent by a signal generator to a power amplifier, operating from Direct Voltage up to the high frequency range (5 MHz),

capable to feed properly the exciting piezo sensors attached to the samples and multiplying by 50 the input voltage. The signal acquired by the receiver piezo sensor was read by an oscilloscope and downloaded to a portable PC (see Figure 2b). A MATLAB code was subsequently used to post-process the signals, in particular, to evaluate the nonlinear metrics and to apply the Fast Fourier Transform. The followed approach consisted in evaluating the frequency content of the acquired signals comparing the responses of the two tested samples. The goal was to find a correlation between the adopted nonlinear metrics and the quality of the adhesion and to find an interpretation to the spectral responses and their nonlinear content.

Nonlinear metrics

Combining the force equilibrium, equation (1), and the linear Hook's law, equation (2), the motion equations can be written as:

$$\frac{\partial \sigma_{ij}}{\partial x_j} = \rho \frac{\partial^2 u_i}{\partial t^2} \tag{1}$$

$$\sigma_{ij} = C_{ijkl} \varepsilon_{kl} \tag{2}$$

where x_j are Lagrangian coordinates, σ_{ij} is the Cauchy stress tensor, u_i the displacement, ε_{kl} the strain, ρ the material density of and C_{ijkl} the fourth-order elasticity tensor. If the wave propagation is assumed longitudinal along the x-direction the linear wave equation is:

$$\frac{1}{c_l^2} \frac{\partial^2 u(x,t)}{\partial t^2} - \frac{\partial^2 u(x,t)}{\partial x^2} = 0 \tag{3}$$

where c_l is the wave propagation speed. A solution of equation (3) as a plane wave oscillating with a harmonic frequency ω is:

$$u(x,t) = u_1 \, sin(k_l x - \omega t) \tag{4}$$

$$u(0,t) = u_0 \, sin(\omega t) = u_0 \, sin(-\omega t) \tag{5}$$

where u_1 is the amplitude of the harmonic wave and k_l is the wave number equal to ω/c_l. It is reasonable to assume for the material a nonlinear elastic behaviour consisting in terms that describe hysteresis, classical nonlinearity and discrete memory. The right-hand side of equation (1) can be expanded into a power series of the strain in $\varepsilon_x = \partial u(x,t)/\partial x$ and its derivatives, which allows for hysteretic phenomena:

$$\begin{aligned}\rho\frac{\partial^2 u(x,t)}{\partial t^2} &= \frac{\partial \sigma_x}{\partial x} + \alpha\left[\Delta\varepsilon_x + \varepsilon_x(t)sign(\dot{\varepsilon}_x)\right] = \frac{\partial \sigma_x}{\partial \varepsilon_x}\frac{\partial \varepsilon_x}{\partial x} + \alpha\left[\Delta\varepsilon_x + \varepsilon_x(t)sign(\dot{\varepsilon}_x)\right] = \\ &= E\frac{\partial}{\partial x}\left[\left(\frac{\partial u(x,t)}{\partial x}\right) + \frac{\beta}{2!}\left(\frac{\partial u(x,t)}{\partial x}\right)^2 + \frac{\gamma}{3!}\left(\frac{\partial u(x,t)}{\partial x}\right)^3 + \cdots\right] + \alpha\left[\Delta\varepsilon_x + \varepsilon_x(t)sign(\dot{\varepsilon}_x)\right]\end{aligned} \tag{6}$$

where $E = \partial\sigma_x/\partial\varepsilon_x$ is the elastic modulus, $\Delta\varepsilon_x$ is the local strain amplitude over a previous wave period, β and γ are higher order nonlinear elastic coefficients, $\dot{\varepsilon}_x = \partial\varepsilon_x/\partial t$ is the strain rate and α is a coefficient related to material hysteresis that in this work is assumed zero. According to the classical nonlinear theory, equation (6) becomes:

$$\frac{\partial^2 u(x,t)}{\partial t^2} = {c_l}^2\frac{\partial^2 u(x,t)}{\partial x^2}\left[1 + \beta\frac{\partial u(x,t)}{\partial x} + \frac{\gamma}{2}\left(\frac{\partial u(x,t)}{\partial x}\right)^2\right] \tag{7}$$

The method adopted to solve equation (7) was based on a perturbation expansion of the displacement in the following form:

$$u(x,t) = u^{(1)}(x,t) + u*(x,t) = u^{(1)}(x,t) + u^{(2)}(x,t) + u^{(3)}(x,t) \tag{8}$$

where the contribution $\left|u^{(1)}(x,t)\right| >> \left|u*(x,t)\right|$ is the solution to the linear wave equation (3) expressed by (4). A first-order perturbation equation for the contribution $u^{(2)}(x,t)$ is obtained substituting expression (8) in (7):

$$\begin{aligned}&\frac{\partial^2 u^{(2)}(x,t)}{\partial t^2} - {c_l}^2\frac{\partial^2 u^{(2)}(x,t)}{\partial x^2} = {c_l}^2\beta\left(\frac{\partial u^{(1)}(x,t)}{\partial x}\right)\left(\frac{\partial^2 u^{(1)}(x,t)}{\partial x^2}\right) \\ &= -\frac{{c_l}^2\beta{k_l}^3{u_1}^2}{2}sin\left[2(k_l x - \omega t)\right]\end{aligned} \tag{9}$$

for which a general solution has the form:

$$u^{(2)}(x,t) = f(x)sin[2(k_x x - \omega t)] + g(x)cos[2(k_x x - \omega t)] \tag{10}$$

After simple transformations and after the application of the proper boundary conditions the solution has the following form:

$$u^{(2)}(x,t) = -\frac{\beta {k_l}^2 {u_1}^2}{8} x\, cos[2(k_l x - \omega t)] \tag{11}$$

where $u_2 = \frac{\beta {k_l}^2 {u_1}^2}{8} x$ is the amplitude of the second harmonic signal. The nonlinear metric β can, therefore, be measured experimentally as a ratio between the second harmonic signal and square of the fundamental multiplied by a constant:

$$\beta = 8\frac{u_2}{{k_l}^2 {u_1}^2 x} \tag{12}$$

The same process can be adopted for evaluating the contribution $u^{(3)}(x,t)$ to the nonlinear wave equation as follows:

$$\begin{aligned} &\frac{\partial^2 u^{(3)}(x,t)}{\partial t^2} - {c_l}^2 \frac{\partial^2 u^{(3)}(x,t)}{\partial x^2} = {c_l}^2 \frac{\delta}{2}\left(\frac{\partial u^{(1)}(x,t)}{\partial x}\right)^2 \left(\frac{\partial^2 u^{(1)}(x,t)}{\partial x^2}\right) \\ &= \frac{{c_l}^2 \gamma {k_l}^4 {u_1}^3}{8}\{-sin(k_l x - \omega t) - sin[3(k_l x - \omega t)]\} \end{aligned} \tag{13}$$

Substituting the general form of the solution in the equation (13) and with the application of the boundary conditions on the third harmonic, the nonlinear parameter γ can be expressed as a ratio between the third harmonic amplitude and the cubic amplitude of the fundamental multiplied by a constant:

$$\gamma = 48\frac{u_3}{{k_l}^3 {u_1}^3 x} \tag{14}$$

Nonlinear oscillator – subharmonic and higher harmonics appearance

The driven motion of a nonlinear oscillator is governed by an equation with the following general form:

$$\ddot{x} + 2\lambda\dot{x} + \omega_o^2 x + \varphi x^2 + \psi x^3 = \frac{F}{m}\cos \nu t \tag{15}$$

where x, $\dot{x}$, and $\ddot{x}$ are the displacement, the velocity and the acceleration functions of the time t, λ is a damping coefficient, ω_0 is the resonant frequency, φ and ψ are coefficients related to the nonlinear forcing terms, F is the driving force, m is the mass, ν is the frequency of the driving force. A solution of this equation can be found as a harmonic function $x(t)=A(v)\cos(vt)$ when the driving force is assumed reasonably small. The response of nonlinear oscillator can be characterized by the appearance of higher harmonics and subharmonics and this remarkable feature has many practical applications. For the superharmonic resonance the input frequency is taken as $\approx \omega_0/n$ and converted into ω_0 via the n-th nonlinearity of the oscillator. Solutions to the (15) originating superharmonic resonance conditions can be found using the perturbation approach [15]. Similarly, subharmonic appearance conditions can occur taking $\nu \approx n\omega_0$ and considering the n-th approximation in (15). Taking $\nu \approx 2\omega_0$, the second approximation in (15) yields:

$$\ddot{x}_2 + 2\lambda\dot{x}_2 + \omega_o^2\left[1 - \frac{2\varphi F}{3m\omega_0^4}\cos\left[(2\omega_0 + \chi)t\right]\right]x_2 = 0 \tag{16}$$

where χ is a frequency perturbation. The equation (16) represents a condition for a subharmonic (fundamental parametric) resonance and its solutions comprise unstable ultra-subharmonic outputs: $\omega_0 = q\nu/2$ (q= 1, 2, 3,…).

Nonlinearities associated to microbubbles in the adhesive

Microbubbles vibrate when excited by acoustic pressure. Their dynamic response is strongly nonlinear depending on their size, on the properties of the medium in which they are located, on their content, and on the boundary conditions. Neglecting surface tension and liquid viscosity and with the assumption of liquid incompressibility, Rayleigh showed from the momentum equation that the bubble boundary (radius), $R(t)$ obeyed the relation:

$$R\ddot{R} + \frac{3}{2}\dot{R}^2 = \frac{p(R) - p_\infty}{\rho} \tag{17}$$

where ρ is the liquid density, p_∞ is the pressure in the liquid at a large distance from the bubble, and *p(R)* is the pressure in the liquid at the bubble boundary. For this Rayleigh problem, *p(R)* is also the pressure within the bubble. Incompressibility of the liquid means that the liquid velocity *w(r,t)* at a distance *r* from the bubble centre is:

$$w(r,t) = \frac{R^2}{r^2}\dot{R} \tag{18}$$

The pressure in the liquid is readily found from the general Bernoulli equation to be:

$$p(r,t) = p_\infty + \frac{R}{r}\left[p(R) - p_\infty\right] + \frac{1}{2}\rho\frac{R}{r}\dot{R}^2\left[1 - \left(\frac{R}{r}\right)^3\right] \tag{19}$$

While Rayleigh neglected surface tension and liquid viscosity and kept the pressure p_∞ constant, his dynamical equation (19) is easily extended to include these effects. For a spherical bubble, viscosity affects only the boundary conditions so that it becomes:

$$p(R) = p_i - \frac{2\sigma^L}{R} - \frac{4\mu}{R}\dot{R} \tag{20}$$

where now p_i is the pressure in the bubble and *p(R)*, as before, is the pressure in the liquid at the bubble boundary. The surface-tension constant and the coefficient of the liquid viscosity are σ^L and μ, respectively. By allowing p_∞ to be a function of time, one can use Equation (17) to describe the experimental observations on cavitation-bubble growth and collapse in a liquid flow [12]. Other effects not considered by Rayleigh, such as the stability of the interface, the compressibility of the liquid, the effect of energy flow into or out of the bubble, and the physical conditions within the bubble, are described and discussed in [12]. A generalized Rayleigh equation for bubble dynamics may be written, in view of Equation (20),

$$R\ddot{R} + \frac{3}{2}\dot{R}^2 = \frac{1}{\rho}\left\{p_i - p_\infty - \frac{2\sigma^L}{R} - \frac{4\mu}{R}\dot{R}\right\} \tag{21}$$

where the pressure in the gas at the bubble wall, p_i, may be a function of the time, and the pressure at infinity, p_∞, may also be a function of the time. Microbubbles vibrating in liquid subjected to harmonic excitation (a sound field) follow the equation (21) that for small amplitude oscillations can be linearized as it follows.

The sound field can be expressed as:

$$p_\infty = P_\infty(1+\delta\cos\omega t) \tag{22}$$

The bubble radius may be written:

$$R = R_0(1+a(t)) \tag{23}$$

The internal pressure $p_i(t)$ can be linearized as it follows:

$$p_i(t) = p_{i,eq} + \left.\frac{\partial p_i}{\partial a}\right|_{a=0,\dot{a}=0} a(t) + \left.\frac{\partial p_i}{\partial \dot{a}}\right|_{a=0,\dot{a}=0} \dot{a}(t) + ... \tag{24}$$

Substituting (22), (23) and (24) in (21), yields:

$$\ddot{a} + 2\beta_g\dot{a} + \omega_{g,0}^2 a = -\delta\alpha_g e^{i\omega t} \tag{25}$$

where the constant α_g is $P_\infty/\rho R_0^2$, the damping constant β_g is:

$$\beta_g = \frac{2\mu}{\rho R_0^2} - \frac{1}{2\rho}\left.\frac{\partial p_i}{\partial \dot{a}}\right|_{a=0,\dot{a}=0} \tag{26}$$

$$\omega_{g,0}^2 = -\frac{1}{\rho}\left.\frac{\partial p_i}{\partial a}\right|_{a=0,\dot{a}=0} - \frac{2\sigma^L}{\rho R_0^3} \tag{27}$$

If the gas is polytropic:

$$p_i = p_{i,eq}\left(\frac{R_0}{R}\right)^{3k} \tag{28}$$

and the natural frequency $\omega_{g,0}$ becomes:

$$\omega_{g,0}^2 = 3k\frac{p_{i,eq}}{\rho R_0^2} - \frac{2\sigma^L}{\rho R_0^3} \tag{29}$$

When the surface tension and viscosity terms in the Rayleigh-Plesset equation are deemed negligible the natural frequency of the bubble becomes:

$$\omega_{g,0}^2 = 3k \frac{p_{i,eq}}{\rho R_0^2} \tag{30}$$

This formula was first derived by Minnaert and for bubbles in water under atmospheric pressure gives:

$$\omega_{g,0} R_0 = 20.49 \cdot Hz \cdot m \tag{31}$$

3. EXPERIMENTAL RESULTS AND DISCUSSION

During the experimental campaign the acquired signals on the Sample 1 and Sample 2 were recorded and post-processed in MATLAB. Their spectral content was carefully analysed. In Figure 3, on the horizontal axis the excitation frequency is represented; on the vertical axis the normalized vibrational amplitude measured by the receiver sensor at the fundamental component (same frequency of the excitation) is reported: the excitation frequency was changed in the chosen range of interest while the voltage amplitude feeding the exciting sensor was kept constant. The information available in this Figure cannot lead to general conclusions about the dynamic properties of the samples (vibrational modes, natural frequencies): the response signal is, indeed, acquired only at one point of the specimen and is related to only one excitation point. The scope of the present work was not the investigation of SLJs' dynamic behaviour under different adhesion conditions, but the analysis of the nonlinearities which appear in their structural response and to find explanations for them. The dynamic behaviour of the samples was found to be very sensitive, according to the expectations, to the adhesive extension that strongly affects their vibrational modes. The response of the Sample 1 shows clear peaks at 27 kHz and 44 kHz. The response of the Sample 2 shows clear peaks at 46 kHz and 48 kHz. Nonlinearities in the structural response of both Samples 1 and 2 were found.

The nonlinear behaviour of Sample 1, which was nominally fully bonded and used as a reference, was unexpected and different interpretations can be provided for this effect that can be correlated to the manufacturing process (contact between the two plates, voids, non-uniformity of the adhesive layer,

inclusions, kissing bond et cetera). In the previous paragraphs the mathematical formulation of metrics able to characterize the nonlinear content of a spectral response was provided and two possible sources of nonlinearities (Contact Acoustic Nonlinearities and microbubbles) were established. The metrics β and γ, characterizing the 2nd and 3rd order harmonic effects on the structural dynamic behaviour of the samples, were evaluated.

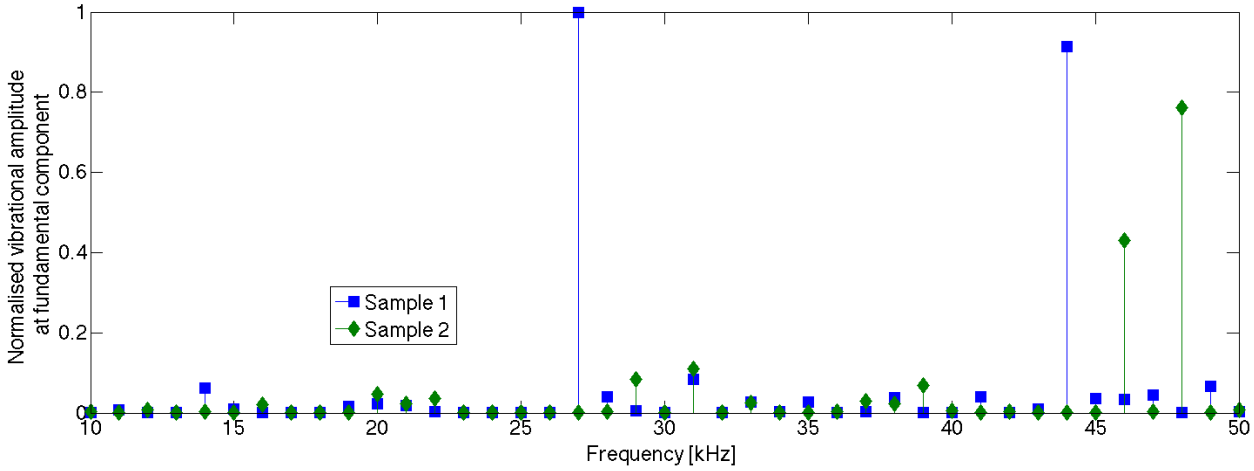

Figure 3. Fundamental component of the structural response for the two configurations investigated

A wide technical discussion about these metrics and their applications in Nonlinear Elastic Wave Spectroscopy can be found in [15]-[20]. Parameter β characterizes the weight of the second harmonic signal respect to the fundamental and was evaluated according to the formula (12): from Figure 4, it is clear that, for both the samples, the spectral content is affected by the appearance of the second harmonic signal. In the range of frequencies chosen for the investigation, nonlinearities appear more pronounced at lower frequencies. Values of the metrics β are higher for Sample 2 than for Sample 1 as expected, and this is verified throughout the entire investigated range. Furthermore, the difference between the same metric applied to the two samples appears more pronounced for excitation frequencies falling in a range between 26 kHz and 45 kHz to which second harmonics correspond in the range between 52 kHz and 90 kHz. Similar conclusions can be reached evaluating the metric γ according to the formula (14), representing the importance

of the third harmonic with respect to the fundamental. From Figure 5 it can be seen that, also in this case, in the frequency range of interest, the metric γ has higher values for Sample 2 than for Sample 1.

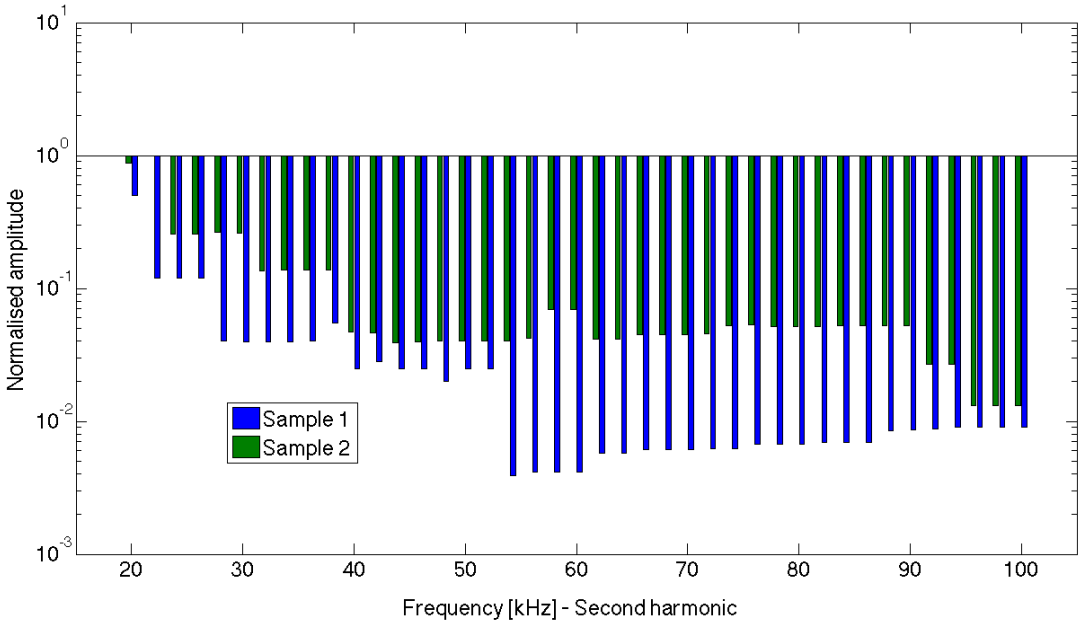

Figure 4. Parameter β evaluated in the frequency range of interest

It is worthwhile remarking that the metrics β and γ, being sensitive to higher order harmonics in the structural spectral response, provide a global indication of nonlinear effects without giving information on the possible reasons for the nonlinearities, neither suggesting possible actions to mitigate nor to cancel these effects. The presence of subharmonics at half of the excitation frequency is another effect noticed in the acquired spectra, not across all of the investigated range but for few frequency values. In Figure 6, the normalized vibrational amplitude of f/2 components, where f is the frequency of the exciting signal, for both the specimens, are reported. Clear peaks at 27 kHz, 35 kHz, 44 kHz can be seen in the Sample 1 spectral response; for the Sample 2 response, peaks were found at 29 kHz, 32 kHz, 35 kHz, 46 kHz, 48 kHz.

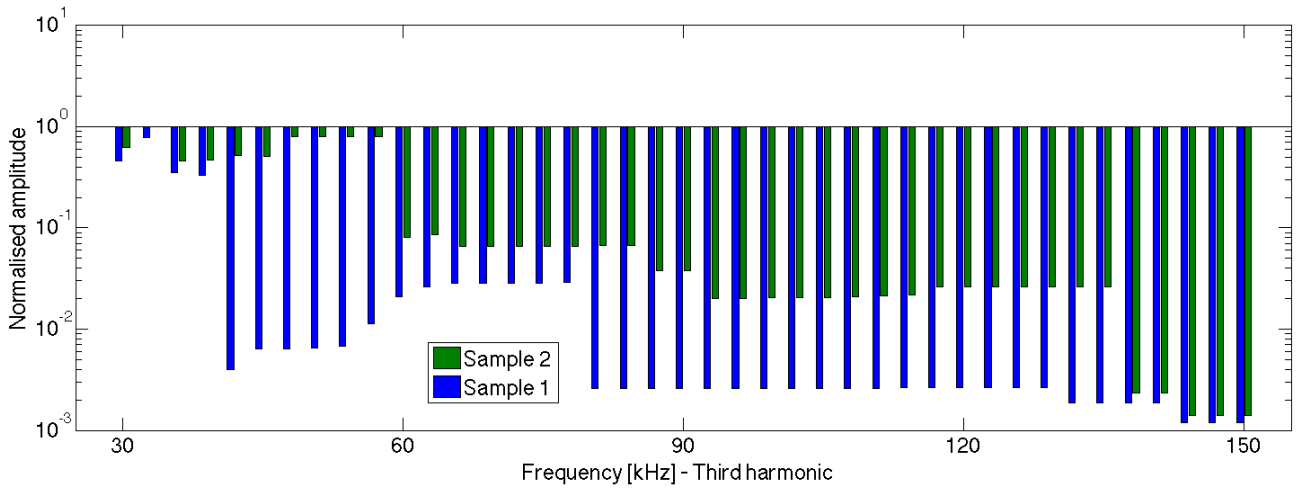

Figure 5. Parameter γ evaluated in the frequency range of interest

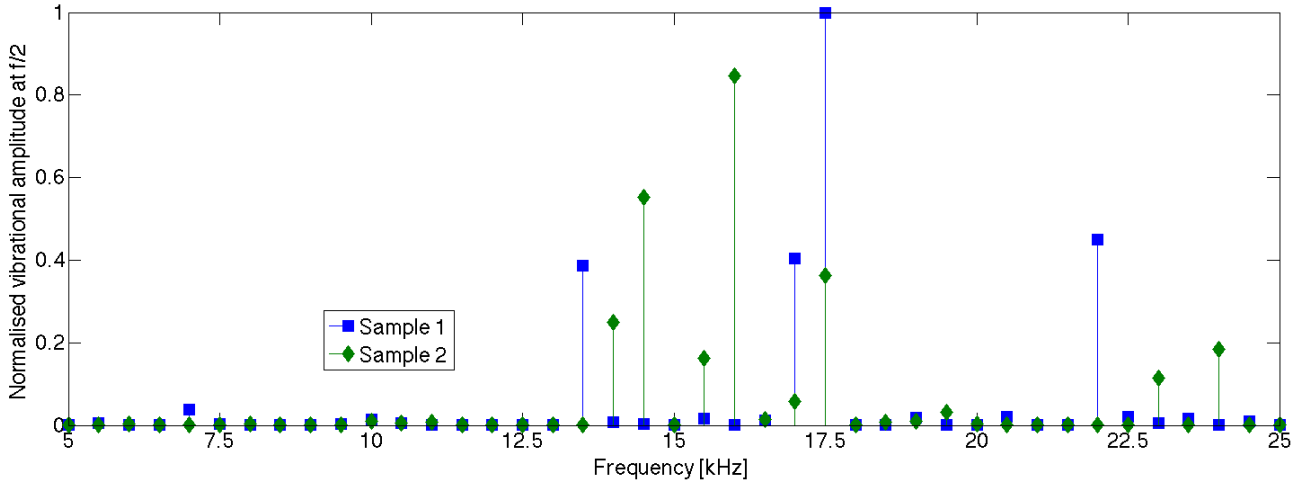

Figure 6. Subharmonic component (f/2) of the structural response for the two configurations investigated

It is worthwhile to analyse the Fast Fourier Transform (FFT) of the signals gathered from the receiver sensors on the specimens. In order to provide possible scientific interpretations of the nonlinearities arising in the structural response of the bonded samples, the possible external causes were initially carefully investigated. In experiments like those presented and discussed in this paper, some nonlinearities can appear due to saturation of the power amplifier response: the operation of the amplifier was, therefore, investigated to exclude the instrumentation as one the possible reasons. Subsequently, different but similar boundary conditions were adopted and carefully investigated in order to exclude the sample support method, used to

constrain the specimens, as the origin of the subharmonics. It was finally concluded that the presence of subharmonics in the spectral response was due to adhesion defects.

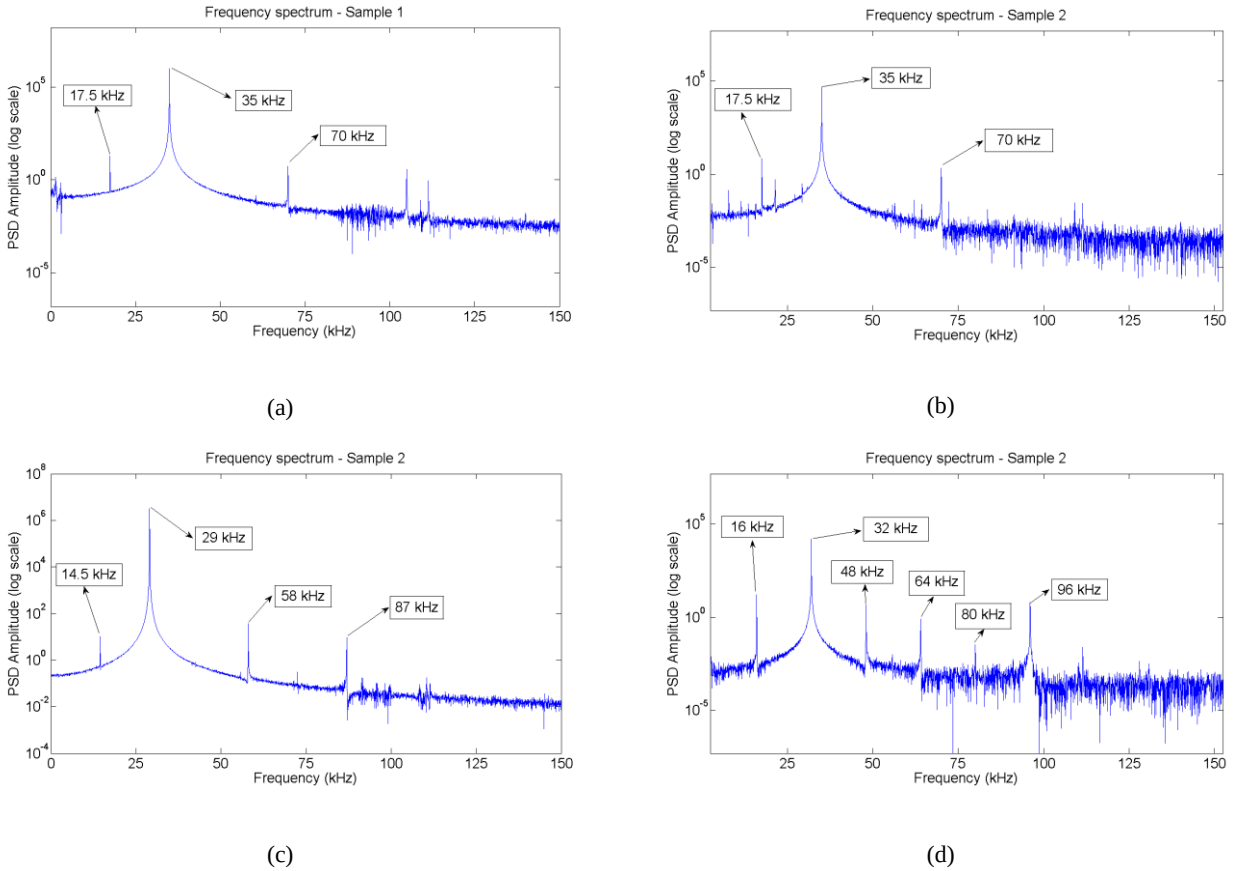

Figure 7. FFT at several frequencies of interest for Sample 1 and Sample 2

The FFTs presented in Figure 7 reveal the presence of a rich variety of harmonics in the response. For Sample 2 an exciting frequency of 32 kHz (see Figure 7d) generates a structural response in which the subharmonic at f/2, 16 kHz, appears together with harmonic components of 48 KHz (3f/2) and 80 kHz (5f/2). The appearance of subharmonics in the behaviour of nonlinear dynamic systems occurs under specific conditions. Generally speaking, nonlinear oscillation systems can be characterized by a rich variety of phenomena in which typical nonlinear spectra are associated with subharmonics and chaos [21]. Crack vibrations can generate acoustic subharmonics [22][23] and a subsequent threshold can be established for the transition to chaotic dynamics for the higher excitations [23][24]. These results confirm that a correlation can be found between an integral damage induced and the subharmonic (and/or “acoustic noise”) level. At the

same time, they do not allow the localization of the flaws in the investigated structure. In [25] it is demonstrated that mechanical defects in solids can produce subharmonics associated with a self-modulation of vibrations, resulting in specific spectrum conversion. Furthermore, both these effects, the presence of subharmonics and the self-modulation of the spectral components, become more pronounced around the defect: in this way, they provide a reliable localization of the damage based on effective imaging techniques.

4. COMPUTED TOMOGRAPHY OF THE SAMPLES

At the University of Bath (Department of Mechanical Engineering), a Nikon XT225H ST X-ray Computed Tomography (CT) system has been used to analyse the bonded samples, to investigate the quality of the adhesion and to provide possible further interpretations of the nonlinearities which arose in both of the samples. The images obtained allowed the identification of porosity in the adhesive layer that is associated with the presence of microbubbles of various dimensions. The microbubbles could explain the presence of subharmonics at different excitation frequencies: it is well known [12][14] that a stable bubble driven in an intense acoustic field emits a subharmonic at half the driven frequency when the bubble is excited near its resonance. In [26] it is demonstrated that if the acoustic pressure increases but the oscillation still remains within the stable regime, the bubbles will oscillate non-linearly and this will result in the appearance of harmonics of the fundamental (nf_0), and weak, often intermittent subharmonic signal ($f_0/2$) and ultra-subharmonics ($(2n+1)f_0/2$). A threshold level of acoustic pressure can be established above which the generation of inertial cavitation is associated with a marked and sudden increase in broadband white noise that is not so intense to mask harmonics and subharmonics that strongly persist. Increasing the intensity through this threshold level, higher-order subharmonics (nf_0/q, $q > n$) appear along with a corresponding set of ultra-subharmonics above the fundamental.

In Figure 8, CT scan images representing sections of two investigated bonded samples are shown: at the top, the fully bonded sample is represented; at the bottom, the partially bonded. It was found that for both the investigated specimens, the adhesive was not uniform in thickness that was far from the nominal thickness (0.15 mm): for the fully bonded specimen the adhesive layer average thickness was thinner (0.13 mm) than

the partially bonded (0.18 mm) and, consequently, a minor content of microbubbles with smaller dimensions was found in it.

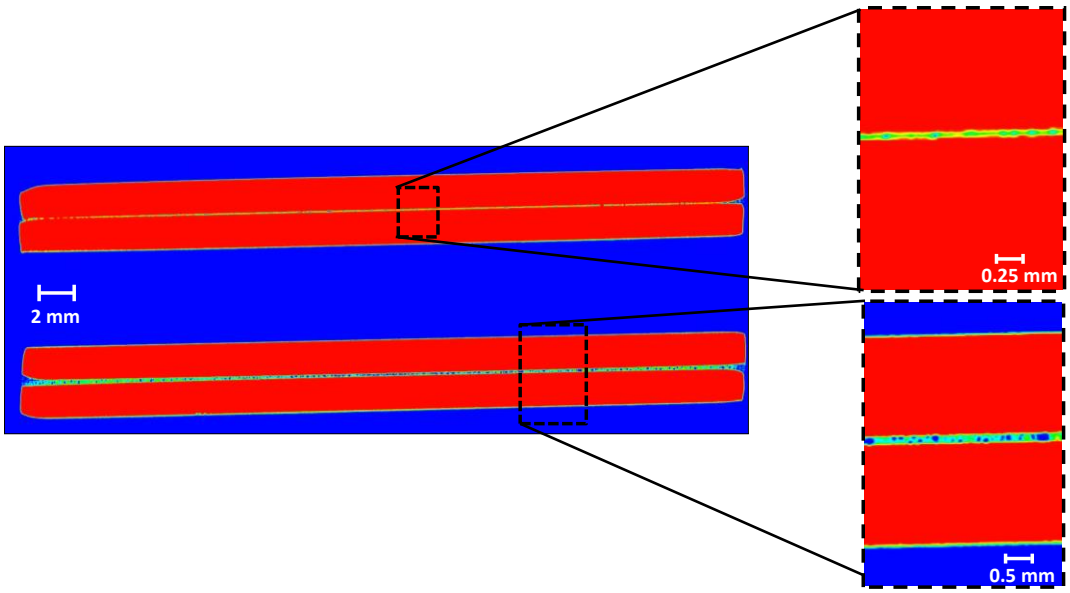

Figure 8. Post-processed CT image of the two bonded samples

Simple evaluations were performed correlating the dimensions of the microbubbles in the adhesive layers revealed by the tomography with the spectral content of the response acquired by the piezo sensors bonded onto the samples. According to formula (30), giving the natural frequency of the microbubbles as a function of their radius, and making the assumption of neglecting the surface tension and the viscosity of the adhesive, using a proper value of its density, the resonance of the microbubbles with radii ranging from 0.015 mm to 0.085 mm falls in the range between 35000 Hz to 198000 Hz. This resonance could be responsible for the spectral content shown in the Figure 7: the use of formula (30) allows one to associate the peaks of the FFTs reported in this Figure with the dimensions that the microbubbles in the adhesive layer should have to promote the subharmonics' appearance (see Table 2).

Sample	Fundamental frequency (kHz)	Microbubbles radius (mm)
1	35	0.0849
2	29	0.1025
2	32	0.0929
2	35	0.0849

Table 2. dimensions of the microbubbles in the adhesive layers matching the subharmonics in the measured spectra

The major limit of this simple approach is the assumption that the cavity inside the adhesive can be properly described by a spherical bubble: this limit could be overcome if a refined acoustical model were developed representing the actual shapes of the cavities/bubbles, the different mediums, the interface between them and the boundary conditions. This possible interpretation of the nonlinearity arisen in the structural response acquired by the receiver sensor during the measurements on the proposed specimens should be carefully verified by designing a specific experiment aimed at characterizing the behaviour of microbubbles in epoxy resins under controlled conditions: a test set-up has been therefore conceived for future research, the design of which is presented here. A controlled number of phenolic resin microspheres of controlled diameters can be dispersed in the adhesive layer between two substrates. The thickness of the adhesive layer and the manufacturing process of the bonded joint should be carefully chosen in order to avoid other nonlinearities (such as kissing bond or contact acoustic nonlinearities). One generator sensor can be bonded onto the top plate and one receiver sensor can be bonded onto the bottom plate. Acoustic pressure fields of different intensities can be generated in order to radiate the microbubbles and their spectral response can be acquired (Figure 9). These experiments are expected to provide confirmation about the influence of the microbubble dynamics on the spectral response of the adhesive joint under harmonic excitation.

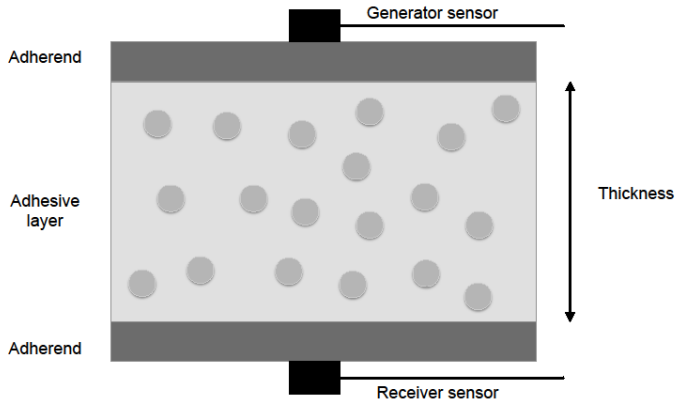

Figure 9. bonded sample aimed at characterizing microbubbles influence on adhesive dynamic response

5. CONCLUSIONS

In this paper two different samples consisting of single lap joints bonded by epoxy resin adhesives were experimentally investigated in order to analyse the nonlinear content of their structural response. Piezo

sensors were bonded onto the specimens that were excited with harmonic loading in the range between 10 kHz and 50 kHz and the spectral response was carefully investigated. Subharmonics and higher order harmonics were found in the measured spectra with different amplitude levels depending on the excitation frequency. The use of specific nonlinear metrics allowed the evaluation of the degree of nonlinearity of the two different samples and, as expected, the partially bonded one exhibited a higher degree of nonlinearity than the fully bonded one: the metrics β and γ, being sensitive to higher order harmonics in the structural spectral response, provide a global indication of nonlinear effects without giving information on the possible reasons for the nonlinearities, neither suggesting possible actions to mitigate nor to cancel these effects. The ultrasounds can be actually employed to establish if the adhesive quality is good or not, leading to the need of more accurate methods to check the adhesive layer: in principle, a threshold of acceptable and low degree of nonlinearity, related to a reference good lap joint, could be established to evaluate the adhesive status. Two possible interpretations of the subharmonic appearance were provided: the first one was based on the contact acoustic nonlinearities; the second one was based on the nonlinear oscillations of the bubbles present in the adhesive layer as suggested by the computed tomography. Further experimental and numerical work is needed to confirm these interpretations.

REFERENCES

[1] Higgins, A.,"Adhesive bonding of aircraft structures, International Journal of Adhesion and Adhesives", Volume 20, Issue 5, 2000, Pages 367-376, ISSN 0143-7496, http://dx.doi.org/10.1016/S0143-7496(00)00006-3.

[2] Kress, G., Naeff, P., Niedermeier, M., Ermanni, P., "The onsert: A new joining technology for sandwich structures", Composite Structures, Volume 73, 2006, Pages 196-207.

[3] Guyott, C.C.H., Cawley P., Adams, R.D., "The non-destructive testing of adhesively bonded structure: a review", Journal of Adhesion, 20:129–159, (1986).

[4] Adams, R. D., Cawley P., "Defect types and non destructive testing techniques for composites & bonded joints", Construction and Building Materials, 3(4):170–183, (1989).

[5] Savage, G., “Failure prevention in bonded joints on primary load bearing structures”, Engineering Failure Analysis, 14:321–348, (2007).

[6] Vine, K., Cawley, P., Kinloch, A. J., “The correlation of non destructive measurements and toughness changes in adhesive joints during environmental attack”, Journal of Adhesion, 77(2):125–161, (2001).

[7] Ehrhart, B., et al., “Methods for the quality assessment of adhesive bonded CFRP structures-a resumé”, Proceedings of 2nd International Symposium on NDT in Aerospace, (2010).

[8] Yan, D., Drinkwater, B.W., and Neild, S.A., “Measurement of the Ultrasonic Nonlinearity of Kissing Bonds in Adhesive Joints,” NDT&E International, Vol. 42, 2009, pp. 459–466.

[9] Yan, D., Drinkwater, B.W., and Neild, S.A., “Experimental and Theoretical Characterization of Kissing Bonds in Adhesive Joint Using Non-Linear Ultrasonic Measurement,” Review of Quantitative Nondestructive Evaluation, Thompson, D.O. and Chimenti, D.E., eds., Vol. 29, 2010, p. 1190–1197.

[10] Yan, D., Drinkwater, B.W., and Neild, S.A., “Modelling and Measurement of the Nonlinear Behaviour of Kissing Bonds in Adhesive Joints,” NDT&E International, Vol. 47, 2012, pp. 18–25. Physics Procedia 70 (2015) 411 – 414

[11] Solodov, I. “Highly-Sensitive Defect-Selective Imaging and NDT via Resonant Nonlinearity of Defects”, 2015 International Congress on Ultrasonics, 2015 ICU Metz, Physics Procedia 70 (2015) 411 – 414.

[12] Plesset, M. S., Prosperetti, A. “Bubble dynamics and cavitation”, Ann. Rev. Fluid Mech, 1977, 9:145-185.

[13] Nayfeh, A. H. “The response of single degree of freedom systems with quadratic and cubic non-linearities to a subharmonic excitation”, Journal of Sound and Vibration (1983) 89(4), 457-470.

[14] Leighton, T. L. et al. “Acoustic Bubble Sizing by Combination of Subharmonic Emissions with Imaging Frequency”, 1991, Ultrasonics 29(4):319-323.

[15] Solodov, I. “Resonant acoustic nonlinearity of defects for highly-efficient nonlinear NDE”, Journal of Nondestructive Evaluation, 33:252-262, (2014).

[16] Ciampa, F., Scarselli, G., & Meo, M. (2015) “Nonlinear imaging method using second order phase symmetry analysis and inverse filtering”, Journal of Nondestructive Evaluation, 34(2), 1-6.

[17] Ciampa, F., Pickering, S., Scarselli, G., Meo, M., “Nonlinear Damage Detection in Composite Structures using Bispectral Analysis”, Proceedings of SPIE - The International Society for Optical Engineering, 906402-8, (doi:10.1117/12.2046631), (2014).

[18] Ciampa, F., Pickering, S., Scarselli, G., Meo, M., "Nonlinear imaging of damage in composite structures using sparse ultrasonic sensor arrays", Structural Control and Health Monitoring, doi: 10.1002/stc.1911, (2016).

[19] Ciampa, F., Onder, E., Barbieri, E., Meo, M., "Detection and Modelling of Nonlinear Elastic Response in Damage Composite Structures", Journal of Nondestructive Evaluation, doi: 10.1007/s10921-014-0247-7, (2014).

[20] Ciampa, F., Barbieri, E., Meo, M., "Modelling of Multiscale Nonlinear Interaction of Elastic Waves with three dimensional cracks", Journal of Acoustical Society of America, 135 (4), doi: 10.1121/1.4868476, (2014).

[21] Minorsky, N., [Nonlinear Oscillations], Van Nostrand, Princeton, (1962).

[22] Solodov, I.Yu., Korshak, B.A., "Instability, chaos and "memory" in acoustic-wave-crack interaction", Physical Review Letters, 88, 014303 (2002).

[23] Moussatov, A., Gusev, V., Castagnede, B., "Self-induced hysteresis for nonlinear acoustic waves in cracked material", Physical Review Letters, 90, 124301 (2003).

[24] Han, X., Li, W., Zeng, Zh., Favro, L.D., Thomas, R.L., "Acoustic chaos and sonic infrared imaging", Applied Physics Letter 81, 3188 (2002).

[25] Solodov, I., Wackerl, J., Pfleiderer, K., Busse, G., "Nonlinear self-modulation and subharmonic acoustic spectroscopy for damage detection and location", Applied Physics Letters 84, 5386, doi: 10.1063/1.1767283, (2004).

[26] Lauterborn, W., Cramer, E., "Sub-harmonic route to chaos observed in acoustics", Phys. Rev. Lett., 47 (20) (1981), p. 1445.